Journal of Hazardous Materials 480 (2024) 136422

Contents lists available at ScienceDirect

Journal of Hazardous Materials

journal homepage: www.elsevier.com/locate/jhazmat

Effect of ocean dynamic processes on the temporal-spatial pattern of persistent organic pollutants (PCB-153 and BDE-47) in the shelf seas

Aobo WANG [a], Xinyu GUO [b,*], Xiaokun DING [c], Jie SHI [d], Jianhui TANG [e], Huiwang GAO [d]

[a] School of Hydraulic and Civil Engineering, Ludong University, Yantai 264025, China
[b] Center for Marine Environmental Studies, Ehime University, Matsuyama 790–8577, Japan
[c] School of Ocean, Yantai University, Yantai 264005, China
[d] Frontiers Science Center for Deep Ocean Multispheres and Earth System, and Key Laboratory of Marine Environment and Ecology, Ministry of Education of China, Ocean University of China, Qingdao 266100, China
[e] Key Laboratory of Coastal Environmental Processes and Ecological Remediation, Yantai Institute of Coastal Zone Research, Chinese Academy of Sciences, Yantai 264003, China

HIGHLIGHTS

- A coupled ocean model was developed to simulate transport of POPs in the shelf seas.
- Ocean dynamic processes can affect the temporal-spatial distributions of POPs.
- The high POP concentration patches at sea surface are related to bottom cold water.
- The prediction function of POP distribution is deduced by numerical experiments.

GRAPHICAL ABSTRACT

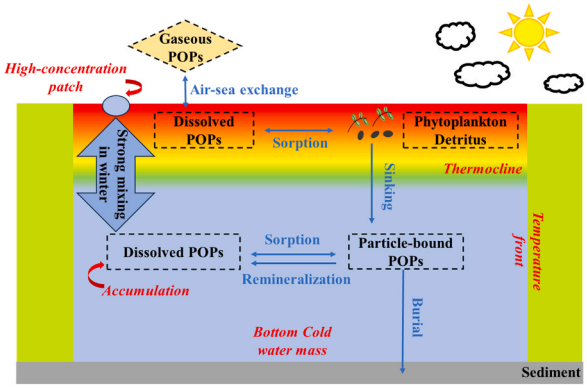

ARTICLE INFO

Keywords:
Coupled model
Bottom cold water mass
Spatial distribution
Persistent organic pollutants
Prediction function

ABSTRACT

Field observations of persistent organic pollutants (POPs) in shelf seas presented abnormal phenomena such as high-concentration patches in offshore areas and different vertical profiles of POPs at the same location. We assumed that these phenomena were associated with the presence of bottom cold water mass (BCWM) in shelf seas and used a hydrodynamic-ecosystem-POP coupled model to confirm this hypothesis. Based on model results, with the formation of BCWM during summer, POPs accumulated inside BCWM due to their transport across the thermocline by the sorption to sinking particles. With the intensification of vertical mixing during winter, the release of POPs from BCWM induced high-concentration patches of POPs on the surface layer. Meanwhile, the low water temperature in winter was favorable for the gas deposition of POPs, which led to high surface concentrations of POPs. Because the accumulation of POPs in BCWM depended on the sorption of dissolved POPs by particles, not all types of POPs accumulated in BCWM. Some POPs even accumulated at the sea surface above the

* Correspondence to: Center for Marine Environmental Studies, Ehime University, 2–5 Bunkyo-Cho, Matsuyama 790–8577, Japan.
E-mail address: guo.xinyu.mz@ehime-u.ac.jp (X. GUO).

https://doi.org/10.1016/j.jhazmat.2024.136422
Received 28 May 2024; Received in revised form 27 October 2024; Accepted 5 November 2024
Available online 7 November 2024

BCWM due to large gaseous deposition and weak sorption by particles. Using this feature, we proposed a prediction function for the accumulation of POPs in BCWM.

1. Introduction

Persistent organic pollutants (POPs) are anthropogenic organic compounds that are difficult to degrade in the environment [1]. POPs have been detected in the wild Antarctic, indicating their long-range transport by the atmosphere and ocean [2]. Furthermore, POPs can accumulate with increasing trophic levels and are highly toxic to animals and humans [3].

Many terrigenous pollutants, including POPs, enter the sea from rivers and the atmosphere [4,5]. The river input and atmospheric aerosol deposition are the main sources of POPs in coastal waters, whereas diffusive air-sea exchange is the dominant source in open seas [6,7]. In seawater, the dissolved POPs are easily absorbed by the biological particles (planktons and detritus, hereafter referred to as "particles" for simplification) due to their hydrophobicity and then experience the same biogeochemical cycles as the particles [4,8].

Air–sea exchange and sorption of POPs by particles are reversible processes that are in dynamic equilibrium in seawater [9,10]. The sorption of POPs by particles and their sinking from surface water can intensify the air-sea exchange flux, which is known as the "biological pump" of POPs in the ocean [11]. Usually, a two-film model is used to calculate the air-sea diffusive fluxes of POPs, which depend on the sea surface temperature (SST), wind speed, Henry's Law Constant of pollutants, and dissolved POP concentrations in air and seawater [12]. The carbon content of the particles is the essence of their sorption of POPs, which includes uptake and adsorption to the matrix and surface of the particles, respectively [8,13]. The depuration and desorption of POPs from particles are the inverse processes of uptake and adsorption [8].

POPs are widely detected in seawater [6,14]. These observations revealed interesting phenomena. For example, dissolved polychlorinated biphenyls (PCBs) and dichlorodiphenyltrichloroethanes (DDTs) in the Greenland Sea have higher concentrations in the lower layer than in the surface layer, with varying vertical gradients [15]. In contrast, hexachlorocyclohexanes (HCHs) have a higher concentration in the surface layer than in the bottom layer of the Greenland Sea [15]. Dissolved DDTs in California coastal waters show a vertical profile similar to that of the Greenland Sea [16].

In addition to the vertical direction, POPs in shelf seas have special features in the horizontal direction. Decabromodiphenyl ether (BDE-209) shows different horizontal patterns in the surface layer and sediment of the Bohai Sea, indicating that its horizontal patterns in the surface and bottom waters are probably different [7]. Besides, some patches with high POP concentrations have been observed in the offshore areas of the Yellow Sea and South China Sea [5,17].

As a physical feature, the stratification of seawater in the shelf sea develops from spring to summer, when there is continuous heat input from the atmosphere [18]. Meanwhile, the tidal currents in shelf seas work against the development of stratification. If the tidal currents are sufficiently strong, stratification cannot occur, and vice versa. Therefore, the spatial variation in tidal currents can induce the appearance of a bottom cold-water mass (BCWM), whose center has the lowest bottom-water temperature in summer [19].

Because of the presence of cold bottom water in shelf seas, we hypothesized that the accumulation and release of POPs in the BCWM are strongly responsible for the spatial distribution of POPs. BCWM appears from spring to summer when the vertical mixing becomes very weak. The dissolved POPs in the surface layer are absorbed by the particles and enter the bottom layer with the sinking of particles [11]. The POPs within the particles can return to their dissolved form along with the remineralization of the particles in the bottom layer [20]. In the presence of BCWM, the dissolved POPs released from the particles are trapped inside the BCWM. The continuous sinking of particles with POPs into the BCWM and the remineralization of particles then induce an accumulation of dissolved POPs inside the BCWM, which may cause different horizontal patterns of POPs in the surface and bottom layers [7]. As the BCWM disappears with the destruction of the stratification in late autumn, the dissolved POPs accumulated in the bottom layer are released into the surface layer, which may be responsible for the observed patches of high POP concentrations in the surface layer [5,21].

To verify the above hypotheses regarding the accumulation and release of POPs in BCWM, we constructed an idealized numerical model to simulate the behavior of POPs associated with BCWM. This study has two goals: quantifying the key processes for the accumulation and release of POPs by the BCWM and finding the necessary conditions for the occurrence of POPs accumulation at the bottom layer. Polychlorinated biphenyl congener 153 (PCB-153) has typical features of POPs, such as hydrophobicity, degradation resistance, and high toxicity [22] and its higher dissolved concentration was detected in the bottom water than in the surface water (Table 1) [15]. We therefore chose it as the first target of the simulations. Moreover, the inverse vertical pattern of another POP, tetrabromodiphenyl ether (BDE-47), was observed in the Yellow Sea during summer (Table 1) [23], which was higher in the surface layer than in the bottom layer. Then, the BDE-47 was selected as the contrast of PCB-153 to find the reasons for their different vertical distributions.

2. Model description

A hydrodynamic-ecosystem-POP coupled model was developed for an idealized shelf sea to simulate the formation and disappearance of the BCWM, as well as the biogeochemical behaviors of POPs related to it.

2.1. Hydrodynamic and ecosystem modules

Seawater pollutants are controlled by ocean dynamics through advection and diffusion. The three-dimensional hydrodynamic module for ocean currents was based on the Princeton Ocean Model [25]. The horizontal grid interval was set to 5 km. The model domain (Fig. 1) contained 51 grids in the zonal direction and 53 grids in the meridional direction, and 21 sigma layers (0.000, −0.002, −0.004, −0.010, −0.020, −0.040, −0.060, −0.080, −0.100, −0.120, −0.140, −0.170, −0.200, −0.300, −0.400, −0.500, −0.650, −0.800, −0.900, −0.950, −1.000) in the vertical direction. In the idealized model domain, the lateral boundary grids were treated as land, and the water depth at all water grids was set to a constant (100 m). The formation of the BCWM during summer depended on the distribution of the vertical eddy diffusivity coefficient [26]. The vertical mixing coefficient at a central circle area (Fig. 1) was calculated by the level 2.5 turbulence closure model, which was affected by surface heat flux and wind stresses [25,27]; the vertical mixing coefficient outside the central circle area was assigned as 0.1 $m^2 \ \ s^{-1}$, which represented a strong vertical mixing. In this configuration, wind stresses were used only to calculate the vertical eddy diffusivity coefficient and did not produce ocean currents.

With the input of surface heat flux from spring to summer, stratification in the central circular area gradually appeared, and the vertical diffusion weakened. Meanwhile, the horizontal difference in the vertical mixing coefficient caused a temperature front between the central circular area and the surrounding area. Consequently, cold water was trapped in the bottom layer of an enclosed space in summer, known as the BCWM. Seasonal variations in surface heat flux and wind speed were assigned as a sine function. The peak value of the heat flux (150 Wm^{-2}) appeared in mid-June, while the trough value (−150 Wm^{-2}) occurred in

mid-December. The strongest wind speed (8 ms^{-1}) occurred in mid-February, whereas the weakest (2 ms^{-1}) occurred in mid-August. The initial values of water temperature, salinity, and current velocity were 8 ℃, 35, and 0 ms^{-1}, respectively.

The ecosystem module was based on the biological model proposed by Fennel et al. [28]. The variables in the ecosystem module included ammonium, nitrate, phytoplankton, zooplankton, small detritus, and large detritus. The initial nitrate value was set to 4.0 $mmolm^{-3}$, while that of the other variables was set to 0.01 $mmolm^{-3}$ [28]. There were no external sources for any of the ecosystem variables. The sum of ammonium and nitrate was referred to as dissolved inorganic nitrogen (*DIN*). The sum of phytoplankton, zooplankton, small detritus, and large detritus were referred to as particles. The biogeochemical cycles of these variables are shown in Fig. S1, and detailed information is provided by Fennel et al. [28]. The ecosystem module was run together with the hydrodynamic module and provided the concentrations of biological variables and the values of some parameters for the calculation of POPs.

2.2. POP module

2.2.1. Transport equations of POPs

The behavior of pollutants in the POP module was calculated based on the hydrodynamic and ecosystem modules (Fig. 2). In the POP module, PCB-153 and BDE-47 had six states: dissolved, phytoplankton-bound, zooplankton-bound, small detritus-bound, large detritus-bound, and gaseous, with concentrations denoted as C_w, C_{wp}, C_{wz}, C_{wsd}, C_{wld}, and C_a, respectively. Here C_{wp} was the sum of POPs adsorbed on the phytoplankton surface (C_{wps}) and that uptake in the phytoplankton matrix (C_{wpm}). Similarly, POPs in other particles were also divided into two parts: one was adsorbed on the surface, and the other was uptake in the matrix. For example, C_{wz} was the sum of C_{wzs} and C_{wzm}; C_{wsd} was the sum of C_{wsds} and C_{wsdm}; C_{wld} was the sum of C_{wlds} and C_{wldm}. In this study, the particle-bound POPs(C_{wpar}) were defined as the sum of POPs in all particles ($C_{wp}+C_{wz}+C_{wsd}+C_{wld}$). C_a was a specified variable that acts as a source of POPs in seawater through the air-sea diffusive flux. The equations for each state of POPs in seawater were as follows.

$$\frac{\partial C_w}{\partial t}+u\frac{\partial C_w}{\partial x}+v\frac{\partial C_w}{\partial y}+w\frac{\partial C_w}{\partial z}=\frac{\partial}{\partial z}\left(K_h\frac{\partial C_w}{\partial z}\right)+D(C_w)+Bio(C_w) \quad (1)$$

$$\frac{\partial C_{wpm}}{\partial t}+u\frac{\partial C_{wpm}}{\partial x}+v\frac{\partial C_{wpm}}{\partial y}+w\frac{\partial C_{wpm}}{\partial z}=\frac{\partial}{\partial z}\left(K_h\frac{\partial C_{wpm}}{\partial z}\right)+D(C_{wpm})+Bio(C_{wpm}) \quad (2)$$

$$\frac{\partial C_{wps}}{\partial t}+u\frac{\partial C_{wps}}{\partial x}+v\frac{\partial C_{wps}}{\partial y}+w\frac{\partial C_{wps}}{\partial z}=\frac{\partial}{\partial z}\left(K_h\frac{\partial C_{wps}}{\partial z}\right)+D(C_{wps})+Bio(C_{wps}) \quad (3)$$

$$\frac{\partial C_{wzm}}{\partial t}+u\frac{\partial C_{wzm}}{\partial x}+v\frac{\partial C_{wzm}}{\partial y}+w\frac{\partial C_{wzm}}{\partial z}=\frac{\partial}{\partial z}\left(K_h\frac{\partial C_{wzm}}{\partial z}\right)+D(C_{wzm})+Bio(C_{wzm}) \quad (4)$$

$$\frac{\partial C_{wzs}}{\partial t}+u\frac{\partial C_{wzs}}{\partial x}+v\frac{\partial C_{wzs}}{\partial y}+w\frac{\partial C_{wzs}}{\partial z}=\frac{\partial}{\partial z}\left(K_h\frac{\partial C_{wzs}}{\partial z}\right)+D(C_{wzs})+Bio(C_{wzs}) \quad (5)$$

$$\frac{\partial C_{wsdm}}{\partial t}+u\frac{\partial C_{wsdm}}{\partial x}+v\frac{\partial C_{wsdm}}{\partial y}+(w+w_{s1})\frac{\partial C_{wsdm}}{\partial z}=\frac{\partial}{\partial z}\left(K_h\frac{\partial C_{wsdm}}{\partial z}\right)+D(C_{wsdm})+Bio(C_{wsdm}) \quad (6)$$

$$\frac{\partial C_{wsds}}{\partial t}+u\frac{\partial C_{wsds}}{\partial x}+v\frac{\partial C_{wsds}}{\partial y}+(w+w_{s1})\frac{\partial C_{wsds}}{\partial z}=\frac{\partial}{\partial z}\left(K_h\frac{\partial C_{wsds}}{\partial z}\right)+D(C_{wsds})+Bio(C_{wsds}) \quad (7)$$

$$\frac{\partial C_{wldm}}{\partial t}+u\frac{\partial C_{wldm}}{\partial x}+v\frac{\partial C_{wldm}}{\partial y}+(w+w_{s2})\frac{\partial C_{wldm}}{\partial z}=\frac{\partial}{\partial z}\left(K_h\frac{\partial C_{wldm}}{\partial z}\right)+D(C_{wldm})+Bio(C_{wldm}) \quad (8)$$

$$\frac{\partial C_{wlds}}{\partial t}+u\frac{\partial C_{wlds}}{\partial x}+v\frac{\partial C_{wlds}}{\partial y}+(w+w_{s2})\frac{\partial C_{wlds}}{\partial z}=\frac{\partial}{\partial z}\left(K_h\frac{\partial C_{wlds}}{\partial z}\right)+D(C_{wlds})+Bio(C_{wlds}) \quad (9)$$

In these equations, t was the time (s); x, y, and z were the zonal, meridional, and vertical coordinates (m); u, v, and w were velocity components in three directions (ms^{-1}); w_{s1} and w_{s2} were sinking velocities (ms^{-1}) of small detritus and large detritus, respectively, and their values were given in Table S1 in Supplementary material; K_h was vertical eddy diffusivity coefficient ($m^2\ \ s^{-1}$); C_w, C_{wps}, C_{wpm}, C_{wzs}, C_{wzm}, C_{wsdm}, C_{wsds}, C_{wldm}, and C_{wlds} were POP concentrations (μgm^{-3}); $D(C_w)$, $D(C_{wps})$, $D(C_{wpm})$, $D(C_{wzs})$, $D(C_{wzm})$, $D(C_{wsds})$, $D(C_{wsdm})$, $D(C_{wlds})$, and $D(C_{wldm})$ were horizontal diffusion terms; $Bio(C_w)$, $Bio(C_{wps})$, $Bio(C_{wpm})$, $Bio(C_{wzs})$, $Bio(C_{wzm})$, $Bio(C_{wsds})$, $Bio(C_{wsdm})$, $Bio(C_{wlds})$, and $Bio(C_{wldm})$ were biogeochemical terms. The biogeochemical terms were described in Appendix A of Supplementary Material. Eqs. (1)–(9) were solved in two steps: an explicit scheme for horizontal and vertical advection, horizontal diffusion, and biogeochemical terms; and an implicit scheme for vertical diffusion.

2.2.2. Source and biogeochemical cycle of POPs

A schematic of the POP module is shown in Fig. 2. Gaseous POPs can enter seawater in their dissolved form through the air-sea interface, whose diffusive flux was specified as the surface boundary condition of dissolved POPs (Eq. (10)). Some of the dissolved POPs decomposed slowly in seawater, while the others were absorbed by the particles and experienced a biogeochemical cycle with those particles. The sorption of POPs by particles was reversible and included uptake and depuration, as well as adsorption and desorption. Biogeochemical processes were calculated using Eq. (S5-S13) and the fluxes in these equations were described in Appendix A. In this system, POPs were removed from seawater by sinking to sediment, and remineralization of particles allowed some of them (80 %) to return to seawater as the bottom

Table 1
The observations of water temperature, ecological variables, and POPs in different seas.

Area/Time	Variable	Vertical Maximum	Vertical Minimum	Vertical Pattern	Ref
Yellow Sea	Temperature (℃)	23	6	Surface>Bottom	[24]
August, 2011	Nitrate ($\mu molL^{-1}$)	8.1	0.1	Surface<Bottom	
	Phytoplankton ($mmolm^{-3}$)	3.3	0.4	Subsurface maximum	
Yellow Sea	BDE−47 (pg L^{-1})	0.32	0.01	Surface>Bottom	[23]
June and August, 2019	BDE−99 (pg L^{-1})	0.19	0.01	Surface<Bottom	
	BDE−153 (pg L^{-1})	0.32	0.01	Surface<Bottom	
Greenland Sea	PCB−44 (fg L^{-1})	50	0.01	Surface<Bottom	[15]
June, 2014-July, 2015	PCB−153 (fg L^{-1})	500	155	Surface<Bottom	

condition of dissolved POPs (Eq. (11)), whereas the remaining (20 %) was buried in the sediment [29,30]. The initial concentrations of POPs in all states were 0 μgm^{-3}. The coupled model was run for eight years to reach a balanced state (Fig. S4), and the model results in the last year were saved for analysis to avoid the influence of initial conditions.

$$k_h \frac{\partial C_w}{\partial z} = F_{aw} \tag{10}$$

$$k_h \frac{\partial C_w}{\partial z} = 0.8 \times F_{sink} \tag{11}$$

Here, F_{aw} ($\mu gm^{-2}\ s^{-1}$) was the air-sea diffusive flux of POPs; F_{sink} ($\mu gm^{-2}\ s^{-1}$) was the sinking flux value of large and small detritus at the sea bottom. The diffusive air-sea exchange of POPs included gaseous deposition and volatilization [12], the flux of which can be calculated as $F_{aw} = k_{aw} \times (C_w - \frac{C_a}{H'})$. The bottom sinking flux was calculated as follows: $F_{sink} = w_{s1} \times (C_{wsdm} + C_{wcds}) + w_{s2} \times (C_{wldm} + C_{wlds})$. In the calculations, the gaseous concentration of POPs (C_a) was fixed as $2.0 \times 10^{-6} \mu gm^{-3}$. The same magnitude of gaseous POP concentrations was observed in marginal seas worldwide [6,31]. H' was the dimensionless Henry's law constant, which was affected by seawater temperature and the enthalpy and entropy during phase change of target POPs [12]; k_{aw} was the mass transfer velocity of POPs between air and sea. The calculations of H' and k_{aw} were given in Appendix A.

3. Results

3.1. Temporal-spatial variations of seawater temperature and ecosystem variables

February, April, August, and November were selected to represent winter, spring, summer, and autumn, respectively. Driven by the surface heat flux, the surface water temperature presented an obvious seasonal variation, which was lowest in February (7 °C) and highest in August (25 °C) (Fig. 3a-d). These seasonal changes were similar to those observed in the mid-latitude seas [26,32]. The model reproduced the evolution of the BCWM, which emerged in spring (Fig. 3a6), intensified in summer (Fig. 3a7), and gradually disappeared from autumn (Fig. 3a8) to winter (Fig. 3a5). The seasonal variation and water temperature difference associated with BCWM were consistent with those observed in realistic seas (Table 1) [24,33]. As shown in Fig. 3a7, the thermocline in summer was approximately 20 m deep and separated the water column into two layers.

The spring phytoplankton bloom and the presence of subsurface maximum concentrations in summer were reproduced using a coupled ecosystem model (Figs. S2a2, a6, a3, and a7). When stratification occurred, the particles were distributed mainly at the sea surface and subsurface, whereas the nutrients maintained a high concentration in the lower layer (Fig. S2). During most of the year, the nitrogen was in a dissolved inorganic state rather than in particles, and the concentrations of phytoplankton and small detritus were higher than those of zooplankton and large detritus. In addition, high-concentration patches of DIN and particles were observed at the sea surface during early winter (Fig. S2a1-e1). The release of DIN from the BCWM owing to intensive vertical mixing was the reason for its high concentration at the sea surface in winter. As for the particles, the high-concentration patch at the surface was mainly caused by the mixing of small detritus particles from the subsurface. The vertical distributions and concentrations of phytoplankton and DIN were close to the field data in the Yellow Sea (Table 1).

Using a thermocline at a depth of 20 m, we separated the water column into upper and lower layers (Fig. 1b). In the upper layer, the DIN concentration was higher in winter than in the other seasons because of the slow growth rate of phytoplankton and the decomposition of particles (Fig. S3). During the spring bloom of phytoplankton, the highest concentrations of phytoplankton appeared in April in the upper layer and supported a high concentration of zooplankton and detritus here (Fig. S3). The concentration of detritus in the lower layer was also higher in April than in other months due to the detritus sinking. Both DIN and particles showed smaller seasonal variation ranges in the lower layer than in the upper layer. The DIN concentration in the lower layer was the highest in summer because of the remineralization of detritus and its accumulation in the BCWM because of weak vertical mixing with the upper layer.

3.2. Temporal and spatial variations of PCB-153

The concentration of dissolved PCB-153 was vertically homogeneous in winter and accumulated in the BCWM from spring to summer (Fig. 4a1-a8). The vertical pattern of dissolved PCB-153 in spring and summer could be verified by the field data of PCB-153 in the Greenland Sea (Table 1), which was much higher in the lower layer than in the upper layer. In addition, the dissolved PCB-153 concentration simulated by our model was of the same magnitude as the observation in the

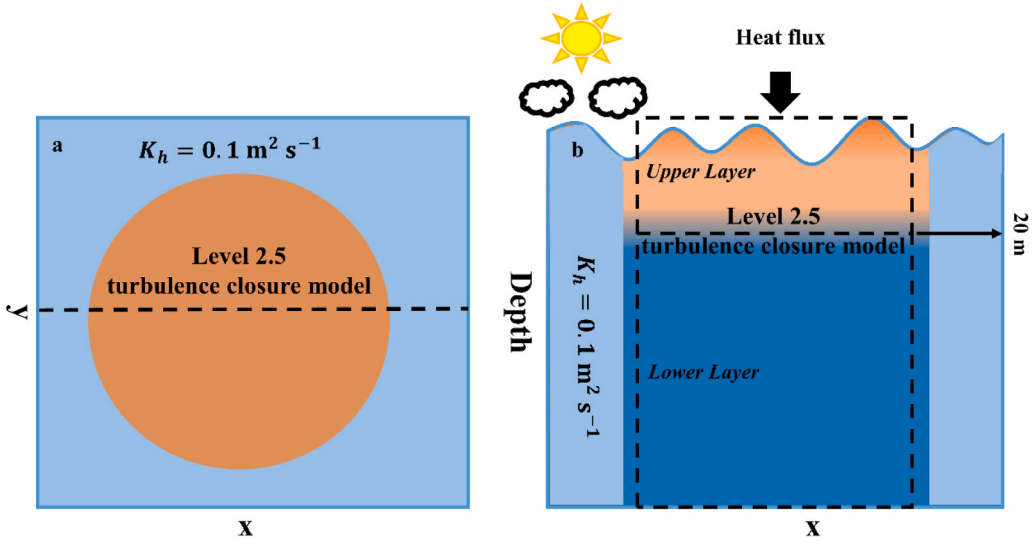

Fig. 1. Top view (a) and lateral view (b) of the model domain. The dashed line in (a) is the location of a section for showing vertical patterns of variables calculated in the model. The dashed box in (b) denotes the upper and lower layers for the area with the bottom cold water mass in summer.

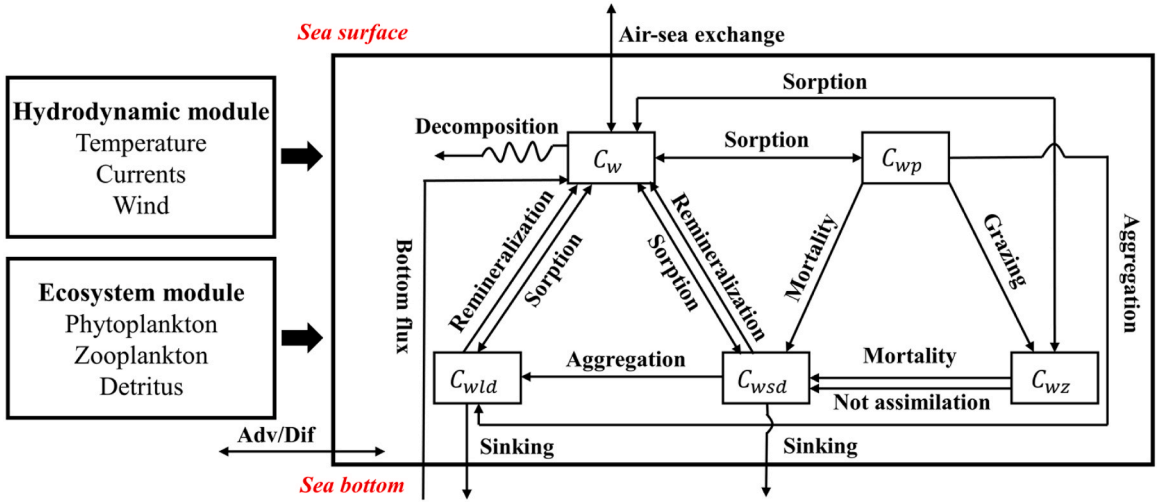

Fig. 2. Conceptual scheme of the hydrodynamic-ecosystem-POP coupled model.

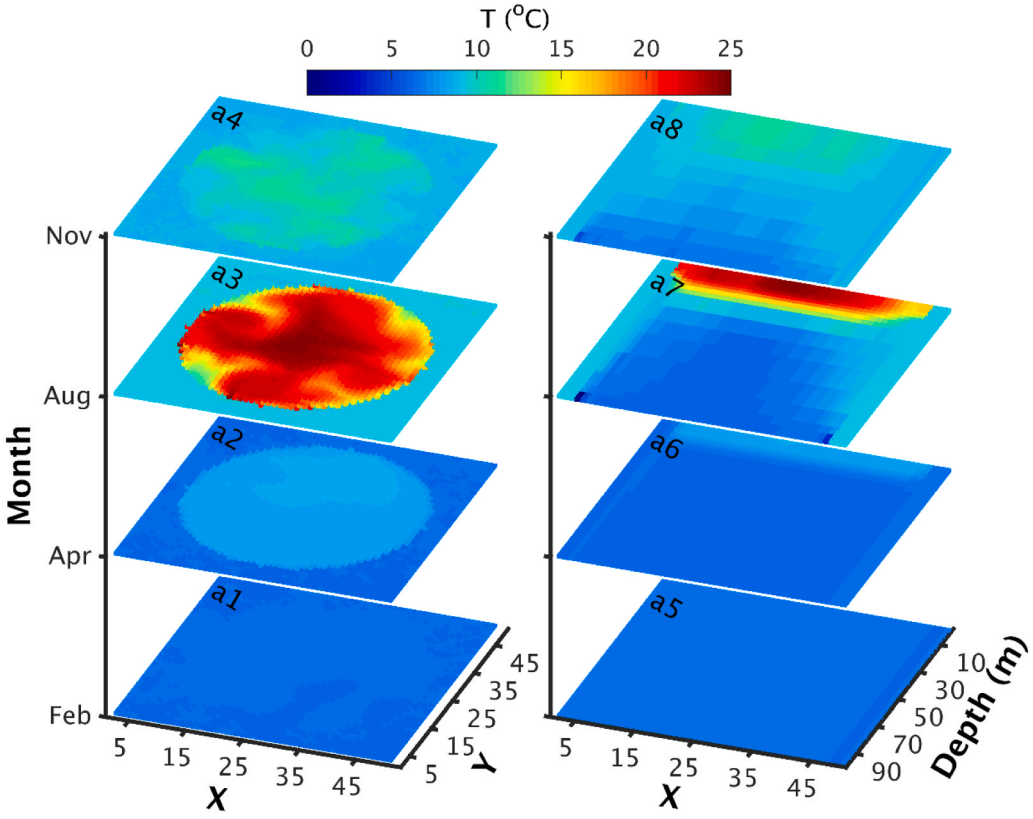

Fig. 3. Horizontal (a1-a4) and vertical (a5-a8) distributions of water temperature in February (a1, a5), April (a2, a6), August (a3, a7), and November (a4, a8).

Greenland Sea (Table 1). When the BCWM was present, the concentration of dissolved PCB-153 in the upper layer was lower in the area above the BCWM than in its surrounding area (Fig. 4a2-a4). However, this horizontal pattern was reversed in the lower layers (Fig. 4a6-a8). This difference was caused by weak and strong vertical mixing in the central and surrounding areas, respectively. Weak vertical mixing induced the presence of dissolved PCB-153 mainly in the lower layer of the central area, whereas strong vertical mixing induced the presence in both the lower and upper layers of the surrounding mixed area. When the BCWM disappeared in February, high-concentration patches of dissolved PCB-153 appeared on the sea surface (Fig. 4a).

The highest concentration of particle-bound PCB-153 appeared in the subsurface in spring and summer (Fig. 4b6-b7), which was consistent with the spatial distribution of the particles. The horizontal patterns of particle-bound PCB-153 also differed in the surface and bottom layers when the BCWM appeared. However, the horizontal difference in its concentration was likely smaller than that of dissolved PCB-153 (Figs. 4b2-b3 and 4b6-b7).

Dissolved PCB-153 had the highest concentration in the upper layer during winter (Fig. S5a) when the input flux from the atmosphere was large [20]. With the sinking and decomposition of particles and the weakening of vertical mixing, it accumulated in the BCWM from spring to summer (Fig. S5a). Particle-bound PCB-153 had the highest concentration in the upper layer in spring because of the spring phytoplankton

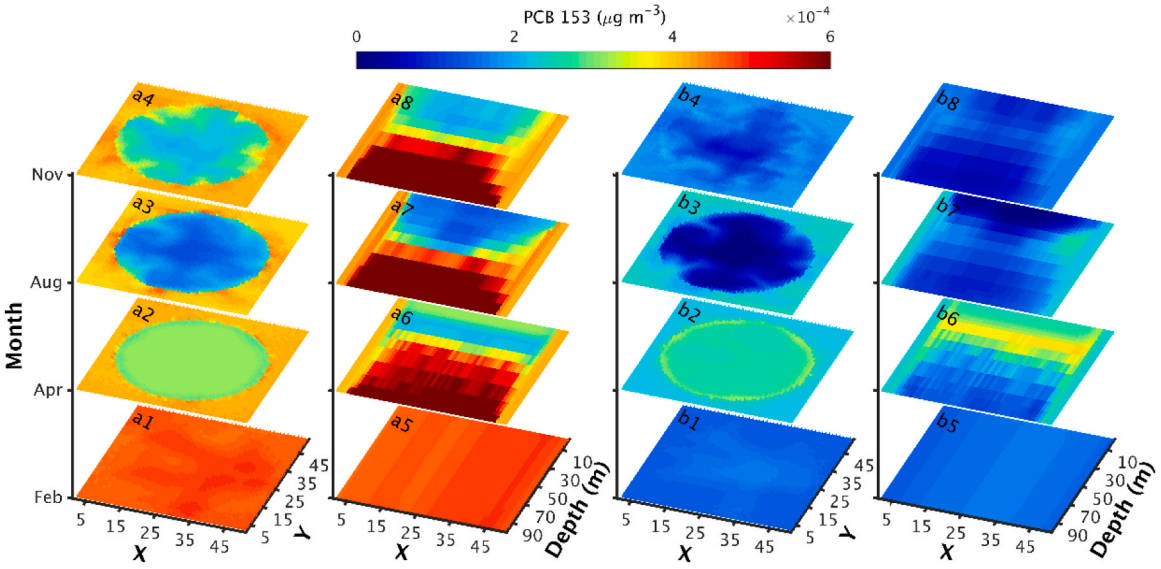

Fig. 4. Horizontal (a1-a4, b1-b4) and vertical (a5-a8, b5- b8) distributions of dissolved (a1-a8) and particle-bound (b1-b8) PCB-153 in February, April, August, and November.

bloom (Fig. S5b); it varied slightly by month in the lower layer, with a higher value in spring than in the other seasons (Fig. S5b).

Interestingly, the temporal variations of dissolved PCB-153 and DIN concentrations were similar whereas those of the particle-bound PCB-153 and particles are also similar. Particle-bound PCB-153 was composed of PCB-153 in phytoplankton, zooplankton, small detritus, and large detritus. The temporal and spatial variations in PCB-153 for each particle type were described in Appendix B.

3.3. Temporal and spatial variations of BDE-47

The dissolved BDE-47 concentration also showed clear vertical variation from spring to autumn (Figs. 5a2-a4), especially during summer, due to the appearance of BCWM. However, the dissolved BDE-47 was accumulated at the surface layer (Fig. 5a3) in summer while the dissolved PCB-153 at the bottom layer (Fig. 5a3). The vertical pattern of dissolved BDE-47 in summer could be verified by the observation of BDE-47 in the Yellow Sea (Table 1). In addition, the horizontal pattern of dissolved BDE-47 was different from that of PCB-153 when the BCWM was present. The dissolved BDE-47 concentration in upper layer was higher in the area above the BCWM than in its surrounding area (Figs. 5a2-a4). The high-concentration patches of dissolved BDE-47 at the central sea surface appeared in spring, summer, and autumn (Figs. 5a2-a4), rather than in winter.

The particle-bound BDE-47 concentration was closely related to the temporal and spatial variations of particle concentrations in seawater, which was higher in spring than in other seasons and was highest at the subsurface vertically in spring and summer (Fig. 5b6-b8). The spatio-temporal pattern of particle-bound BDE-47 was similar to particle-bound PCB-153, but the ratio of particle-bound BDE-47 concentration to dissolved BDE-47 concentration was smaller than that of PCB-153 due to the less lipophilicity of BDE-47.

The spatially averaged concentrations of dissolved and particle-bound BDE-47 were also calculated in the upper and lower layers, respectively. The dissolved BDE-47 concentration was highest in June in upper layer (Fig. S6a) due to the accumulation of dissolved BDE-47 at the sea surface caused by the weak vertical diffusion. In the lower layer, the dissolved BDE-47 concentration was higher in winter than in other seasons (Fig. S6b), which was caused by the intensive vertical diffusion of dissolved BDE-47 accumulated at the upper layer. As described above, the seasonal variations of dissolved BDE-47 in the upper and lower layers were quite different from those of dissolved PCB-153. As for particle-bound BDE-47, its concentrations were highest in April in both the upper and lower layers due to the spring bloom of phytoplankton (Fig. S6), which was similar to the concentration of particle-bound PCB-153.

The particle-bound BDE-47 included those in phytoplankton, zooplankton, small detritus, and large detritus. The seasonal and spatial patterns of BDE-47 in different particles were similar to that of PCB-153 (Fig. S8), which was described in Appendix B.

4. Discussion

4.1. Budget of PCB-153 in the upper and lower layers

The budget of POPs referred to the calculation of spatial-temporally integrated POP fluxes through boundary and those of the source and sink processes, in a given seawater volume and during a specified period. In addition, the balanced budget of POPs in seawater meant that the total change of POP mass was equal to the sum of integrated POP fluxes through the boundary and those of the source and sink processes. Therefore, the budget calculation results were able to quantitatively understand the transport and biogeochemical cycle of POPs in seawater.

To understand the material flow associated with BCWM and identify the key processes for the different vertical distributions of POPs during summer, we calculated the mass budget of PCB-153 (Figs. 5 and 6) and BDE-47 (Fig. 7) in the upper and lower layers. Because accumulation and release occurred in different seasons, the budgets of POPs were given for the period from March to May (warm season) and from November to the next January (cold season). The detailed equations for the budget calculation were presented in Appendix C.

Dissolved PCB-153 accumulated in the bottom layer from March to May, when BCWM formed, indicated by 158.9 g increase in the lower layer. Meanwhile, there was 93.4 g decrease in the dissolved PCB-153 mass in the upper layer. The decrease in dissolved PCB-153 in the upper layer was mainly caused by its transfer from seawater to particles (221.1 g) (Fig. 6a). The increase in dissolved PCB-153 in the lower layer was mainly caused by the transfer from the particles to the dissolved phase (173.9 g) (Fig. 6a). In addition, the sinking of particles was an important mechanism for PCB-153 to move from the upper to the lower layer (276.4 g) (Fig. 6a). Therefore, the key processes for the accumulation of dissolved PCB-153 in the BCWM included sorption of PCB-153 by particles in the upper water, sinking of particles from the upper layer to the lower layer, and remineralization of the particles in the lower

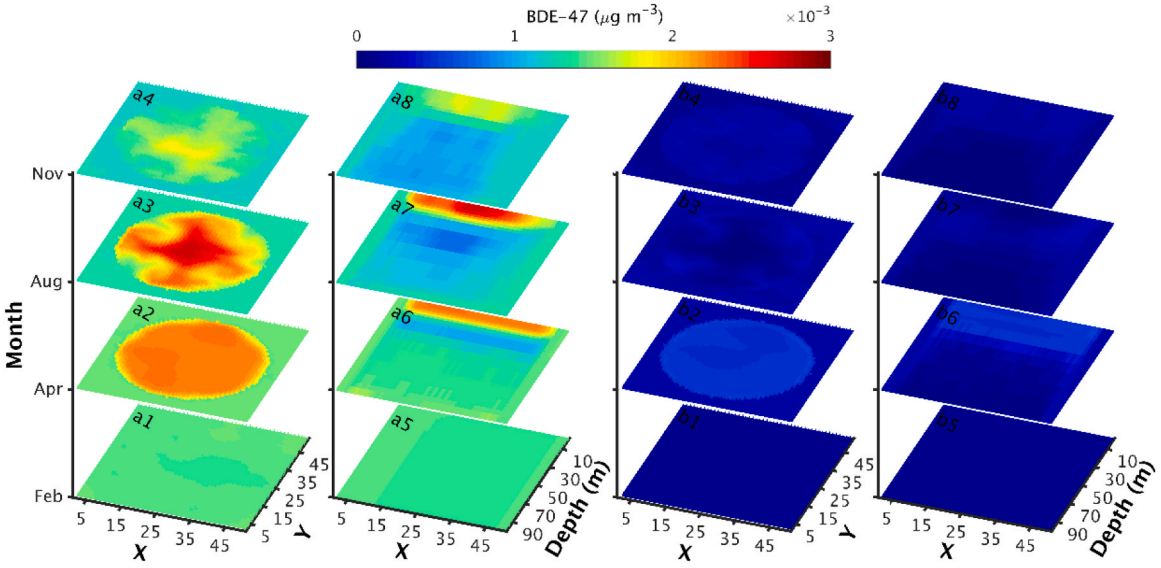

Fig. 5. Horizontal (a1-a4, b1-b4) and vertical (a5-a8, b5- b8) distributions of dissolved (a1-a8) and particle-bound (b1-b8) BDE-47 in February, April, August, and November.

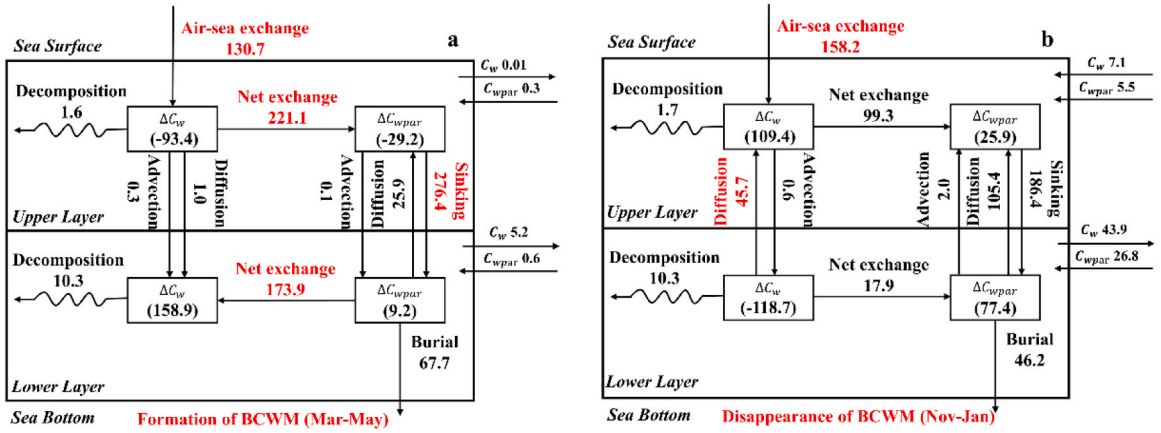

Fig. 6. Mass budget of PCB-153 during the period from March to May (a) and the period from November to next January (b). The unit of integral PCB-153 flux in every process is gram. The upper and lower layers are defined as dashed boxes in Fig. 1b.

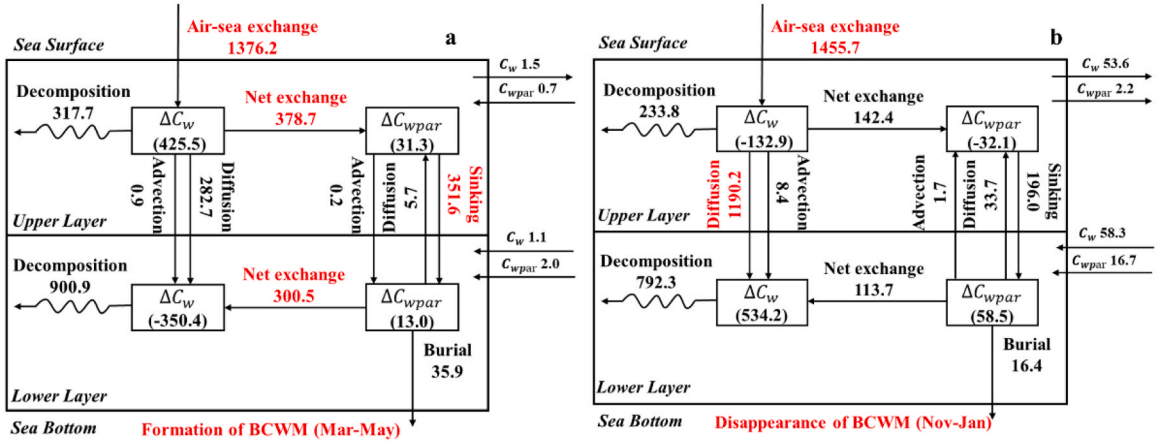

Fig. 7. Mass budget of BDE-47 during the period from March to May (a) and the period from November to next January (b). The unit of integral BDE-47 flux in every process is gram. The upper and lower layers are defined as dashed boxes in Fig. 1b.

water (Fig. 6a), which was a typical pattern of "biological pump" of POPs. The advection and diffusion of PCB-153 in both the vertical and horizontal directions were insignificant as compared with the processes mentioned above from March to May (Fig. 6a).

The vertical diffusion of dissolved PCB-153 (45.7 g) (Fig. 6b) was an important process responsible for the appearance of high-concentration patches on the sea surface in February. Air–sea exchange (158.2 g) also contributed to an increase in dissolved PCB-153 in the upper layer (Fig. 6b). There were two reasons for the large air-sea exchange flux of PCB-153 from November to January. One was the concentration difference of PCB-153 between air and sea, which was large in the earlier stage of November because the presence of "biological pump" of POPs kept a low concentration of dissolved PCB-153 at the sea surface. The other was low surface water temperature, which led to a large fugacity of PCB-153 from the air to the sea [12]. The integrated exchange flux of PCB-153 through the lateral boundary was higher in winter than in spring. The large horizontal gradient of PCB-153 concentration likely increased the horizontal diffusion flux in winter. In Fig. 6, PCB-153 for all particles was put together and shown. The details of the transformation of PCB-153 among different particles were described in Appendix D.

In addition to the time integration of the PCB-153 fluxes shown in Fig. 6, the time series of the PCB-153 fluxes for the key processes were also presented (Fig. S11). The PCB-153 fluxes of sorption to particles in the upper water, sinking of particles from the upper layer to the lower layer, and remineralization of particles in the lower layer were highest in spring, consistent with the phytoplankton bloom (Fig. S11a-b). The air-to-sea flux of PCB-153 was also the highest in spring (Fig. S11a) when sorption to particles reduced the dissolved PCB-153 concentration in seawater and increases the concentration difference between air and sea. The large fluxes of PCB-153 in these four processes during spring indicated that the spring phytoplankton bloom was an important process for the accumulation of PCB-153 in the BCWM. In addition, the vertical mixing fluxes were high in winter (Fig. S11c). Consequently, the dissolved PCB-153 that accumulated in the lower layer moved to the upper layer, leading to the appearance of high-concentration patches of PCB-153.

4.2. Budget of BDE-47 in the upper and lower layers

The calculation equations for budget and fluxes through biogeochemical processes of BDE-47 were the same as those of PCB-153. The dissolved BDE-47 was accumulated at the sea surface rather than at the sea bottom when the BCWM existed (Fig. 5b2-b4), given by 425.5 g increase in the upper layer and 350.4 g decrease in the lower layer (Fig. 7a). Based on the budget result, the accumulation of dissolved BDE-47 in the upper layer was mainly caused by the large air to sea flux (Fig. 7a). In addition, the sorption of dissolved BDE-47 by particles was not so intense as the process of PCB-153 (Fig. 7a). As a result, abundant BDE-47 from the atmosphere could not be transported to lower layer through the sinking of particles and accumulated at sea surface when the BCWM formed. Similar to PCB-153, the horizontal advection and diffusion through the lateral boundary of BDE-47 were not so significant compared with other biogeochemical processes from March to May (Fig. 7a).

Based on the budget of BDE-47 during the disappearance period of BCMW, a mass of dissolved BDE-47 was transported from the sea surface to the bottom (Fig. 7b) due to the enhanced vertical diffusion, which led to the increase of dissolved BDE-47 concentration in the lower layer (Fig. 7b). As analyzed above, the sorption of BDE-47 by particles was not so intense, so the decomposition became the important fate process of dissolved BDE-47 in the seawater (Fig. 7).

Comparing the budget of PCB-153 and BDE-47, the air to sea flux of PCB-153 was much smaller than that of BDE-47 in both the formation and disappearance period of the BCWM (Fig. 6 and Fig. 7), although their concentrations in the atmosphere were set as the same values in the model. The difference between PCB-153 and BDE-47 in the air-sea exchange flux was related to their different Henry's Law Constant (H). The larger H value of PCB-153 led to its higher fugacity from sea to air compared with BDE-47, so the input of PCB-153 from the atmosphere was lower. Moreover, the POP lipophilicity was related to the bioconcentration factor (BCF) of POPs, and the larger BCF of PCB-153 led to the higher fugacity from seawater to particles compared with BDE-47. As a result, for dissolved PCB-153, the weak input from the atmosphere and intense transport by particles from the upper layer to the lower layer contributed to its accumulation at the sea bottom (Fig. 6). On the contrary, for dissolved BDE-47, the large input from atmosphere and weak transport by sinking particles (Fig. S12) led to its accumulation at the sea surface (Fig. 7).

4.3. Impact factors on accumulation of POPs in BCWM

Based on the model results of PCB-153 and BDE-47 described in Sections 3.2–3.3 and observations of POPs in different seawater (Table 1), it can be indicated that different types of POPs present different vertical distributions of concentrations when a thermocline exists. As a result, not all types of POPs accumulated in the BCWM. Therefore, determining the accumulation of POPs in the BCWM is a critical issue. As shown by the budget of PCB-153 and BDE-47, the accumulation of POPs at the sea bottom or the surface when the BCWM was presented was mainly affected by two processes: the diffusive air-sea exchange flux and the sorption of POPs by the particles. The diffusive air-sea exchange of POPs included gaseous deposition and volatilization, which were related to the H of POPs [12]. The small and large values of H indicated the intensive gaseous deposition and volatilization processes of POPs, respectively. The large value of H led to intensive fugacity of POPs from the seawater to the atmosphere. The sorption of POPs by particles was affected by the POP's BCF. The larger BCF was, the stronger sorption was [8]. In other words, the large value of BCF led to intensive fugacity of POPs from the seawater to the particles and promoted the "biological pump" of POPs, which was favorable to the accumulation of POPs in the BCWM. Therefore, it was possible to predict the accumulation of POPs in the BCWM using the H and BCF as predictor variables. In addition, the vertical distribution of POPs was also affected by other POP properties such as half-lives and solubilities although the H and BCF were the key parameters related to the "biological pump" of POPs in a certain BCWM area. This study focused on the effects of H and BCF on the POP vertical distribution, representing the initial step toward the theoretical prediction of POP accumulation in the BCWM area.

As shown in budget results (Fig. 6 and Fig. 7), the ratio of the variation in the spatially mean pollutant concentration (variations in pollutant mass per unit volume) during the formation period of the BCWM in the upper layer to that in the lower layer can be used as an index to quantify the accumulation in the BCWM. Here, the variation in the pollutant concentration was the sum of the dissolved and particle-bound pollutants. The pollutant concentration variation in the upper layer can be estimated by the air-sea flux and sinking flux to the lower water, whereas that in the lower layer was estimated by the sinking flux from the upper water and burial flux. The four fluxes mentioned above were related to the H and the BCF of POPs. As a result, the ratio of variation in pollutant concentration in the upper layer to that in the lower layer can be represented by H and BCF of one certain POP as Eq. (12), which was defined as accumulation ratio (α), whose detailed derivation was given in appendix E.

$$\alpha = \frac{r_1 \times BCF + r_2 \times H + r_3}{r_4 \times BCF + r_5 \times H} \tag{12}$$

Here r_1-r_5 were undetermined constants related to the water temperature and concentrations of particles.

To fit the prediction function of α based on H and BCF, we carried out a series of calculations for POPs with different H and BCF values. A total of 35 sets of calculations were designed for five values of H and seven

values of *BCF* (Fig. S15). These cases were designed for different values of *H* and *BCF*, some of which did not correspond to realistic pollutants. In these calculations, the other biogeochemical parameters were the same as those used in the PCB-153 calculation. As shown in Fig. S15, in the presence of BCWM, the concentration was higher in the surface layer than in the bottom layer for POPs with small *H* and *BCF*. With the increase in *H* and *BCF*, the concentration of POPs in the bottom layer increased, and POPs accumulated in the BCWM.

The accumulation ratios in these cases were calculated using Eq. (S42). Moreover, the undetermined constants and α in Eq. (12) were obtained using the *H* and *BCF* used in these cases (Table S2). With the obtained values of the constants, a prediction function for the accumulation ratio of POPs in the BCWM during summer was established with the specified *H* and *BCF*, which approximately captured the primary features of the model results (Fig. 8). Some accumulation ratios of realistic POPs with varying *H* and *BCF* were presented in Fig. 8, which was helpful to understand the prediction results. The predicted accumulation ratios of realistic POPs, such as BDE-99 and BDE-153 (Fig. 8), can match well with the observed data (Table 1). The critical value of α for the accumulation of POPs in the BCWM was 1. The critical values of *H* and *BCF* were also calculated from critical α. As shown in Fig. 8, the concentrations of POPs will be higher in the upper water than in lower water during summer when *H* is smaller than 7.8 and *BCF* is smaller than 250.0; the accumulation of POPs in the BCWM need a condition that *H* is larger than 7.8 or *BCF* is larger than 250.0.

5. Conclusions

Interesting spatial patterns of POPs in ocean water have been observed, such as high-concentration patches on the sea surface and different vertical distributions of different POPs in the same area. The POPs are easily absorbed by particles in the euphotic layer due to their hydrophobicity and then transferred to the lower layer through the sinking of particles, known as the "biological pump" of POPs. We hypothesized that special phenomena were caused by the accumulation and release of POPs in the BCWM from the perspective of ocean dynamics. A hydrodynamic-ecosystem-POP coupled model was established for an idealized sea to investigate how the BCWM affects the temporal-spatial patterns of POPs in seawater and the conditions for the occurrence of special phenomena. The BCWM in summer, as well as the spring bloom and summer subsurface maximum values of phytoplankton, were reproduced by the coupled model and were of the same magnitude as those observed in the shelf waters. The accumulation of dissolved PCB-153 in the BCWM in summer and its high-concentration patches in winter were predicted by the coupled model. In addition, the different spatiotemporal variations of BDE-47 from PCB-153 were simulated by the model. The biogeochemical cycles of PCB-153 and BDE-47 in the seawater were quantified based on their budgets in the upper and lower layers. The sorption of PCB-153 by particles in the upper layer, sinking with particles, and remineralization of particles in the lower layer were key processes responsible for the accumulation of pollutants in the BCWM, and the intensive vertical mixing and air-sea exchange of PCB-153 in winter were key processes for the high-concentration patches at the surface. The accumulation of BDE-47 at the sea surface in summer was caused by its large fugacity from the atmosphere to the seawater and weak fugacity from the seawater to the particles. Both the model results and observations indicated that not all POPs accumulated in the BCWM, and the accumulation ratio was defined to describe this process. A dependent relationship between the accumulation ratio and the values of *H* and *BCF* was obtained from the model results for a series of POPs. The critical accumulation ratio was deduced from the occurrence of POP accumulation in the BCWM, and the critical values of *H* and *BCF* were determined.

The temporal and spatial variations of POPs in the BCWM area are influenced by both the intensity of thermocline, particle concentration in seawater, and various POP characteristics, such as lipophilicity, volatility, half-lives, and solubilities. However, this study focuses primarily on the lipophilicity and volatility of POPs, as these are the key factors affecting the "biological pump" of POPs in a certain BCWM area. This focus causes that the prediction function for accumulation ratio is not universally applicable to different POPs across various BCWMs, which represents a limitation of this work. Utilizing the POP lipophilicity and volatility as predictor variables is the initial step toward theoretically predicting the POP accumulation in BCWM area. In future

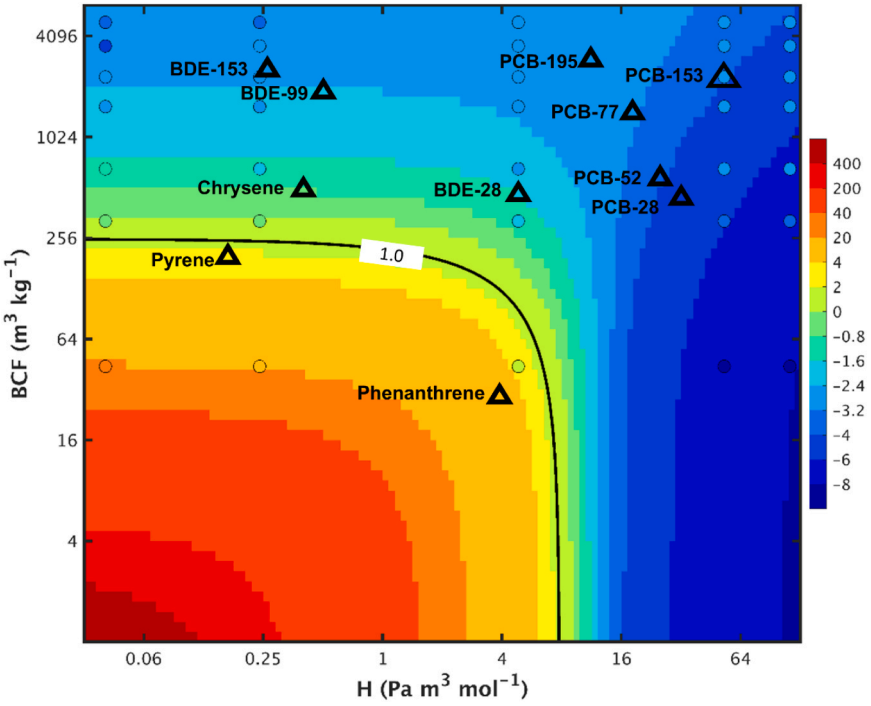

Fig. 8. Prediction of accumulation ratios in BCWM of POPs with different Henry's law constants and bioconcentration factors. Dots with black cycles represent model results. Triangles represent the predicted accumulation ratios of some realistic POPs.

work, we plan to incorporate intensity of thermocline, particle concentration in seawater, and other properties of POPs such as half-lives and solubilities into the prediction function.

Environmental implication

Persistent organic pollutants (POPs) are easy to bioconcentrate and threaten human health due to their high toxicity. The ocean is an important pool of POPs originating from land and the bottom cold water in the ocean can capture POPs for the weak material exchange between cold water and surrounding water. The capture process is related to POP biochemical features. The universal prediction function for the vertical distributions of any kind of POPs in the bottom cold water is beneficial to protect the safety of marine cold-water farming and human health.

Declaration of Competing Interest

The authors declare that they have no known competing financial interests or personal relationships that could have appeared to influence the work reported in this paper.

Acknowledgments

This study is funded by the National Nature Science Foundation of China (41976013, 42406008) , a Grant-in-Aid for Scientific Research (MEXT KAKENHI, Grant 20KK0239), and Sasakawa fund of the Japan Science Society (No. 2021-2028). This work is also supported by the Ministry of Education, Culture, Sports, Science and Technology, Japan (MEXT) to a project on Joint Usage/Research Center–Leading Academia in Marine and Environment Pollution Research (LaMer). X. Ding thanks the Yantai University Start-up Foundation (HX22B109) for supporting his work.

Appendix A. Supporting information

Supplementary data associated with this article can be found in the online version at doi:10.1016/j.jhazmat.2024.136422.

Data Availability

The authors do not have permission to share data.

References

[1] Hao, Z., Xu, H., Feng, Z., Zhang, C., Zhou, X., Wang, Z., et al., 2021. Spatial distribution, deposition flux, and environmental impact of typical persistent organic pollutants in surficial sediments in the Eastern China Marginal Seas (ECMSs). J Hazard Mater 407, 124343. https://doi.org/10.1016/j.jhazmat.2020.124343.

[2] Isla, E., Pérez-Albaladejo, E., Porte, C., 2018. Toxic anthropogenic signature in Antarctic continental shelf and deep sea sediments. Sci Rep 8, 1–7. https://doi.org/10.1038/s41598-018-27375-4.

[3] Hoondert, R.P.J., Van Den Brink, N.W., Van Den Heuvel-Greve, M.J., Ragas, A.M. J., Jan Hendriks, A., 2020. Implications of trophic variability for modeling biomagnification of POPs in marine food webs in the svalbard archipelago. Environ Sci Technol 54, 4026–4035. https://doi.org/10.1021/acs.est.9b06666.

[4] Alekseenko, E., Thouvenin, B., Tronczyński, J., Carlotti, F., Garreau, P., Tixier, C., et al., 2018. Modeling of PCB trophic transfer in the Gulf of Lions; 3D coupled model application. Mar Pollut Bull 128, 140–155. https://doi.org/10.1016/j.marpolbul.2018.01.008.

[5] Zhang, Z.M., Zhang, H.H., Zou, Y.W., Yang, G.P., 2018. Distribution and ecotoxicological state of phthalate esters in the sea-surface microlayer, seawater and sediment of the Bohai Sea and the Yellow Sea. Environ Pollut 240, 235–247. https://doi.org/10.1016/j.envpol.2018.04.056.

[6] Wu, Z., Lin, T., Guo, T., Li, Y., Li, Z., Guo, Z., 2020. Occurrence, air-sea exchange, and gas-particle partitioning of atmospheric polybrominated diphenyl ethers from East Asia to the Northwest Pacific Ocean. Chemosphere 240, 124933. https://doi.org/10.1016/j.chemosphere.2019.124933.

[7] Zhen, X., Li, Y., Tang, J., Wang, X., Liu, L., Zhong, M., et al., 2021. Decabromodiphenyl ether versus decabromodiphenyl ethane: source, fate, and influencing factors in a Coastal Sea Nearing Source Region. Environ Sci Technol. https://doi.org/10.1021/acs.est.0c08528.

[8] Del Vento, S., Dachs, J., 2002. Prediction of uptake dynamics of persistent organic pollutants by bacteria and phytoplankton. Environ Toxicol Chem 21, 2099–2107. https://doi.org/10.1002/etc.5620211013.

[9] Gioia, R., Lohmann, R., Dachs, J., Temme, C., Lakaschus, S., Schulz-Bull, D., et al., 2008. Polychlorinated biphenyls in air and water of the North Atlantic and Arctic Ocean. J Geophys Res Atmospheres 113, 1–11. https://doi.org/10.1029/2007JD009750.

[10] Wang, A., Guo, X., Shi, J., Luo, C., Gao, H., 2019. A simulation of the seasonal variation of decabromodiphenyl ether in a bay adjacent to the Yellow Sea. Sci Total Environ 664, 522–535. https://doi.org/10.1016/j.scitotenv.2019.01.385.

[11] Galbán-Malagón, C.J., Berrojalbiz, N., Gioia, R., Dachs, J., 2013. The “degradative” and “biological” pumps controls on the atmospheric deposition and sequestration of hexachlorocyclohexanes and hexachlorobenzene in the North Atlantic and Arctic Oceans. Environ Sci Technol 47, 7195–7203. https://doi.org/10.1021/es4011256.

[12] Cetin, B., Odabasi, M., 2005. Measurement of Henry’s law constants of seven polybrominated diphenyl ether (PBDE) congeners as a function of temperature. Atmos Environ 39, 5273–5280. https://doi.org/10.1016/j.atmosenv.2005.05.029.

[13] Sobek, A., Gustafsson, Ö., Hajdu, S., Larsson, U., 2004. Particle-water partitioning of PCBs in the photic zone: a 25-month study in the open baltic sea. Environ Sci Technol 38, 1375–1382. https://doi.org/10.1021/es034447u.

[14] Meng, J., Hong, S., Wang, T., Li, Q., Yoon, S.J., Lu, Y., et al., 2017. Traditional and new POPs in environments along the Bohai and Yellow Seas: an overview of China and South Korea. Chemosphere 169, 503–515. https://doi.org/10.1016/j.chemosphere.2016.11.108.

[15] Ma, Y., Adelman, D.A., Bauerfeind, E., Cabrerizo, A., McDonough, C.A., Muir, D., et al., 2018. Concentrations and water mass transport of legacy POPs in the Arctic Ocean. Geophys Res Lett 45, 12,972–12,981. https://doi.org/10.1029/2018GL078759.

[16] Fernandez, L.A., Lao, W., Maruya, K.A., White, C., Burgess, R.M., 2012. Passive sampling to measure baseline dissolved persistent organic pollutant concentrations in the water column of the Palos Verdes shelf superfund site. Environ Sci Technol 46, 11937–11947. https://doi.org/10.1021/es302139y.

[17] Zheng, H., Gao, Y., Xia, Y., Yang, H., Cai, M., 2020. Seasonal variation of legacy organochlorine pesticides (OCPs) From East Asia to the Arctic Ocean. Geophys Res Lett 47. https://doi.org/10.1029/2020GL089775.

[18] Rozema, P.D., Biggs, T., Sprong, P.A.A., Buma, A.G.J., Venables, H.J., Evans, C., et al., 2017. Summer microbial community composition governed by upper-ocean stratification and nutrient availability in northern Marguerite Bay, Antarctica. Deep Sea Res 2 Top Stud Oceano 139, 151–166. https://doi.org/10.1016/j.dsr2.2016.11.016.

[19] Hill, A.E., Brown, J., Fernand, L., Holt, J., Horsburgh, K.J., Proctor, R., et al., 2008. Thermohaline circulation of shallow tidal seas. Geophys Res Lett 35. https://doi.org/10.1029/2008GL033459.

[20] Wang, A., Guo, X., Ding, X., Shi, J., Tang, J., 2024. Effect of hydrodynamic and ecosystem conditions on persistent organic pollutant temporal-spatial variations in the Yellow Sea. J Hazard Mater, 134051. https://doi.org/10.1016/j.jhazmat.2024.134051.

[21] Chen, Z., Qiao, F., Xia, C., Wang, G., 2015. The numerical investigation of seasonal variation of the cold water mass in the Beibu Gulf and its mechanisms. Acta Oceanol Sin 34, 44–54. https://doi.org/10.1007/s13131-015-0595-x.

[22] Li, Q., Xu, Y., Li, J., Pan, X., Liu, X., Zhang, G., 2012. Levels and spatial distribution of gaseous polychlorinated biphenyls and polychlorinated naphthalenes in the air over the northern South China Sea. Atmos Environ 56, 228–235. https://doi.org/10.1016/j.atmosenv.2012.03.074.

[23] Chen, Y., Wang, A., Tang, J., 2024. Spatial distribution, seasonal variation and ecological risk of brominated flame retardants in the seawater of the South Yellow Sea, China. Geochimica, available online. https://doi.org/10.19700/j.0379–1726.2024.01.121 (in Chinese with English abstract).

[24] Fu, M., Sun, P., Wang, Z., Wei, Q., Qu, P., Zhang, X., et al., 2018. Structure, characteristics and possible formation mechanisms of the subsurface chlorophyll maximum in the Yellow Sea Cold Water Mass. Cont Shelf Res 165, 93–105. https://doi.org/10.1016/j.csr.2018.07.007.

[25] Mellor, G.L., Häkkinen, S.M., Ezer, T., Patchen, R.C., 2002. A generalization of a sigma coordinate ocean model and an intercomparison of model vertical grids. In: Pinardi, N., Woods, J. (Eds.), Ocean Forecasting: Conceptual Basis and Applications. Springer, Berlin, pp. 55–72. https://doi.org/10.1007/978-3-662-22648-3_4.

[26] Zhu, J., Shi, J., Guo, X., Gao, H., Yao, X., 2018. Air-sea heat flux control on the Yellow Sea Cold Water Mass intensity and implications for its prediction. Cont Shelf Res 152, 14–26. https://doi.org/10.1016/j.csr.2017.10.006.

[27] Huang, C.J., Qiao, F., Song, Z., Ezer, T., 2011. Improving simulations of the upper ocean by inclusion of surface waves in the Mellor-Yamada turbulence scheme. J Geophys Res Oceans 116, 1–13. https://doi.org/10.1029/2010JC006320.

[28] Fennel, K., Wilkin, J., Levin, J., Moisan, J., O’Reilly, J., Haidvogel, D., 2006. Nitrogen cycling in the Middle Atlantic Bight: Results from a three-dimensional model and implications for the North Atlantic nitrogen budget. Glob Biogeochem Cycles 20. https://doi.org/10.1029/2005GB002456.

[29] Burdige, D.J., 2007. Preservation of organic matter in marine sediments: controls, mechanisms, and an imbalance in sediment organic carbon budgets? Chem Rev 107, 467–485. https://doi.org/10.1021/cr050347q.

[30] Su, B., Pahlow, M., Oschlies, A., 2016. Box-modelling of the impacts of atmospheric nitrogen deposition and benthic remineralisation on the nitrogen cycle of the eastern tropical South Pacific. Biogeosciences 13, 4985–5001. https://doi.org/10.5194/bg-13-4985-2016.

[31] Pegoraro, C.N., Harner, T., Su, K., Chiappero, M.S., 2016. Assessing levels of POPs in air over the South Atlantic Ocean off the coast of South America. Sci Total Environ 571, 172–177. https://doi.org/10.1016/j.scitotenv.2016.07.149.
[32] García-Corral, L.S., Barber, E., Regaudie-De-Gioux, A., Sal, S., Holding, J.M., Agustí, S., et al., 2014. Temperature dependence of planktonic metabolism in the subtropical North Atlantic Ocean. Biogeosciences 11, 4529–4540. https://doi.org/10.5194/bg-11-4529-2014.
[33] Matthew, B., Alkire Eric D'Asaro, Mary Jane Perry, Nathan Briggs, Ivona Cetinić, Amanda Gray, C.L., 2014. Seasonal migration of the Yellow Sea bottom cold water. J Geophys Res Oceans 119, 6121–6139. https://doi.org/10.1002/2014JC009873. Received.